J|A|C|S
A R T I C L E S

What Controls the Melting Properties of DNA-Linked Gold Nanoparticle Assemblies?

Rongchao Jin, Guosheng Wu, Zhi Li, Chad A. Mirkin,* and George C. Schatz*

Contribution from the Department of Chemistry and Institute for Nanotechnology, Northwestern University, 2145 Sheridan Road, Evanston, Illinois 60208

Received August 16, 2002 ; E-mail: camirkin@chem.northwestern.edu; schatz@chem.northwestern.edu

Abstract: We report a series of experiments and a theoretical model designed to systematically define and evaluate the relative importance of nanoparticle, oligonucleotide, and environmental variables that contribute to the observed sharp melting transitions associated with DNA-linked nanoparticle structures. These variables include the size of the nanoparticles, the surface density of the oligonucleotides on the nanoparticles, the dielectric constant of the surrounding medium, target concentration, and the position of the nanoparticles with respect to one another within the aggregate. The experimental data may be understood in terms of a thermodynamic model that attributes the sharp melting to a cooperative mechanism that results from two key factors: the presence of multiple DNA linkers between each pair of nanoparticles and a decrease in the melting temperature as DNA strands melt due to a concomitant reduction in local salt concentration. The cooperative melting effect, originating from short-range duplex-to-duplex interactions, is independent of DNA base sequences studied and should be universal for any type of nanostructured probe that is heavily functionalized with oligonucleotides. Understanding the fundamental origins of the melting properties of DNA-linked nanoparticle aggregates (or monolayers) is of paramount importance because these properties directly impact one's ability to formulate high sensitivity and selectivity DNA detection systems and construct materials from these novel nanoparticle materials.

Introduction

Nanoparticles heavily functionalized with oligonucleotides have been used as probes in a variety of DNA detection methods and as elemental building blocks in materials synthesis schemes based upon the sequence-specific hybridization properties of DNA.[1-9] Detection methods that rely on these materials show promise with respect to increased selectivity and sensitivity as compared with many conventional assays that rely on molecular probes.[10-26] In the case of target selectivity, the nanoparticle

probes can be used to differentiate perfectly complementary targets from those with single-base mismatches, whereas the analogous assays based upon molecular fluorophores do not offer such selectivity. The origin of this selectivity derives, in part, from the extraordinarily sharp melting profiles exhibited by duplex DNA structures formed between target strands of DNA and the nanoparticle probes in the context of aggregate structures or single nanoparticle probes hybridized to capture DNA strands immobilized on a glass slide, Scheme 1A and B and Figure 1. In the case of aggregate structures, the transition is even sharper when visualized with the naked eye via a procedure which involves spotting a solution containing the aggregate as a function of solution temperature on a reverse phase silica gel plate, compare Figure 1A−C. Because these observations directly impact one's ability to formulate high selectivity DNA detection systems and construct materials from

(1) Mirkin, C. A.; Letsinger, R. L.; Mucic, R. C.; Storhoff, J. J. *Nature* **1996**, *382*, 607.
(2) Alivisatos, A. P.; Johnsson, K. P.; Peng, X.; Wilson, T. E.; Loweth, C. J.; Bruchez, M. P.; Schultz, P. G. *Nature* **1996**, *382*, 609.
(3) Mucic, R. C.; Storhoff, J. J.; Mirkin, C. A.; Letsinger, R. L. *J. Am. Chem. Soc.* **1998**, *120*, 12674.
(4) Winfree, E.; Liu, F.; Wenzler, L. A.; Seeman, N. C. *Nature* **1998**, *394*, 539.
(5) Mann, S.; Shenton, W.; Li, M.; Connolly, S.; Fitzmaurice, D. *Adv. Mater.* **2000**, *12*, 147.
(6) Elghanian, R.; Storhoff, J. J.; Mucic, R. C.; Letsinger, R. L.; Mirkin, C. A. *Science* **1997**, *277*, 1078.
(7) Taylor, J. R.; Fang, M. M.; Nie, S. *Anal. Chem.* **2000**, *72*, 1979.
(8) Cui, Y.; Wei, Q.; Park, H.; Lieber, C. M. *Science* **2001**, *293*, 1289.
(9) Nicewarner-Peñña, S. R.; Freeman, R. G.; Reiss, B. D.; He, L.; Peñña, D. J.; Walton, I. D.; Cromer, R.; Keating, C. D.; Natan, M. J. *Science* **2001**, *294*, 137.
(10) Storhoff, J. J.; Elghanian, R.; Mucic, R. C.; Mirkin, C. A.; Letsinger, R. L. *J. Am. Chem. Soc.* **1998**, *120*, 1959.
(11) Taton, T. A.; Mucic, R. C.; Mirkin, C. A.; Letsinger, R. L. *J. Am. Chem. Soc.* **2000**, *122*, 6305.
(12) Niemeyer, C. M.; Ceyhan, B.; Gao, S.; Chi, L.; Peschel, S.; Simon, U. *Colloid Polym. Sci.* **2001**, *279*, 68.
(13) Shipway, A. N.; Willner, I. *Chem. Commun.* **2001**, 2035.
(14) He, L.; Musick, M. D.; Nicewarner, S. R.; Salinas, F. G.; Benkovic, S. J.; Natan, M. J.; Keating, C. D. *J. Am. Chem. Soc.* **2000**, *122*, 9071.
(15) Reichert, J.; Csaki, A.; Kohler, J. M.; Fritzsche, W. *Anal. Chem.* **2000**, *72*, 6025.

(16) Souza, G. R.; Miller, J. H. *J. Am. Chem. Soc.* **2001**, *123*, 6734.
(17) Dujardin, E.; Hsin, L. B.; Wang, C. R. C.; Mann, S. *Chem. Commun.* **2001**, 1264.
(18) Lin, L.; Zhao, H. Q.; Li, J. R.; Tang, J. A.; Duan, M. X.; Jiang, L. *Biochem. Biophys. Res. Commun.* **2000**, *274*, 817−820.
(19) Authier, L.; Grossiord, C.; Brossier, P. *Anal. Chem.* **2001**, *73*, 4450.
(20) Patolsky, F.; Ranjit, K. T.; Lichtenstein, A.; Willner, I. *Chem. Commun.* **2000**, 1025.
(21) Han, S.; Lin, J.; Satjapipat, M.; Baca, A. J.; Zhou, F. *Chem. Commun.* **2001**, 609.
(22) Zhou, X. C.; O'Shea, S. J.; Li, S. F. *Chem. Commun.* **2000**, 953.
(23) Wang, J.; Polsky, R.; Xu, D. *Langmuir* **2001**, *17*, 5739.
(24) Cai, H.; Xu, C.; He, P. G.; Fang, Y. Z. *J. Electroanal. Chem.* **2001**, *510*, 78.
(25) Limoges, B. *Anal. Chem.* **2001**, *73*, 4450.
(26) Dubertret, B.; Calame, M.; Libchaber, A. J. *Nat. Biotechnol.* **2001**, *19*, 365.
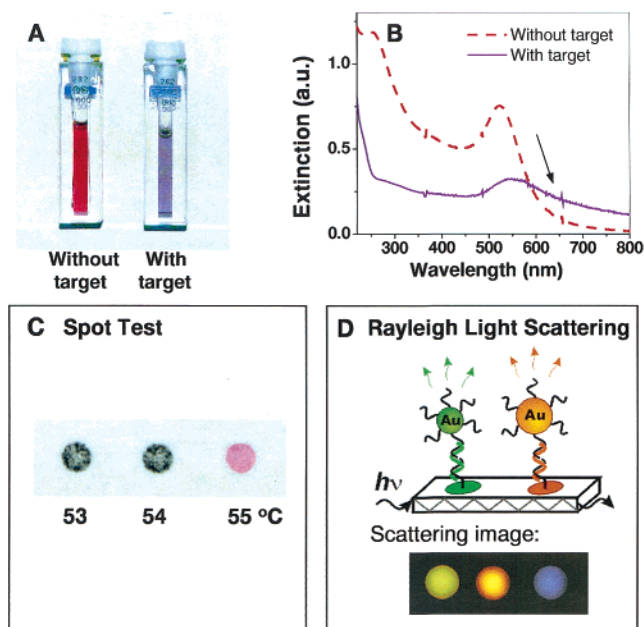
Figure 1. (A) The colorimetric response for Au nanoparticle probes after adding target. (B) UV−vis spectra of nanoparticle probes without target (dash line) and with target (solid line). (C) Spot tests for the target-linked nanoparticle aggregates show an extremely narrow melting range (13 nm diameter Au particles were used). (D) Rayleigh light-scattering from different size and composition nanoparticles on a glass chip: green = Au 50 nm, orange = Au 100 nm, and purple = Ag 40 nm (coated with a monolayer of gold).

Scheme 1
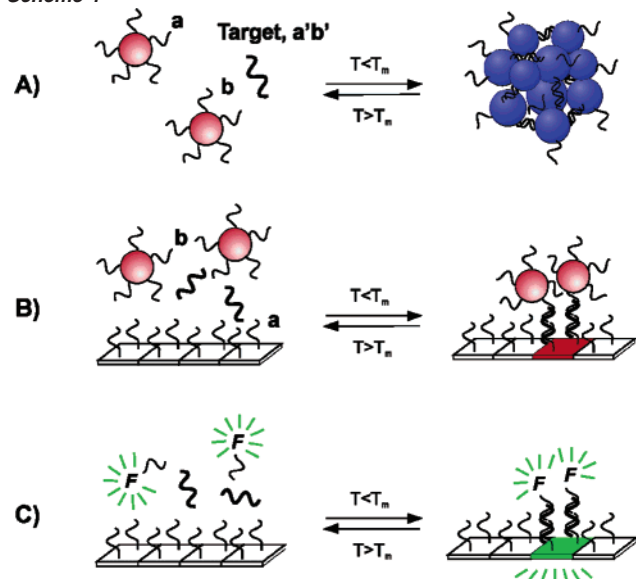
these novel nanoparticle materials, it is essential that the fundamental origins of the melting properties be elucidated.

Herein, we describe a series of experiments and theoretical modeling designed to systematically define and evaluate the relative importance of nanoparticle and experimental variables that contribute to the observed sharp melting transitions. These variables include the size of the nanoparticles, the surface density of the oligonucleotides on the nanoparticles, the dielectric constant of the surrounding medium, target concentration, and the position of the nanoparticles with respect to one another within the aggregate. We will show that the experimental data may be understood in terms of a thermodynamic model that

Table 1. Oligonucleotides Used in the Melting Experiments[a]

	base sequence
a	3′ HS-A$_{20}$-CTC CCT AAT AAC AAT 5′
b	3′ TTA TAA CTA TTC CTA-A$_{20}$-SH 5′
target, **a′b′**	5′ GAG GGA TTA TTG TTA AAT ATT-GAT AAG GAT 3′
diluent strand **1**	3′ HS-A$_{20}$ 5′
diluent strand **2**	3′ A$_{20}$-SH 5′

[a] Spacer A$_{20}$ = AAA AAA AAA AAA AAA AAA AA; diluent strands are only used in the surface density studies.

attributes the sharp melting to a cooperative mechanism that results from two key factors: the presence of multiple DNA linkers between each pair of nanoparticles and a decrease in the melting temperature as duplex DNA strands melt due to a concomitant reduction in local dielectric.

Results

Assay Formats. The nanoparticle probes have been used in two different general formats to detect single-strand oligonucleotide targets. The first format involves the use of two nanoparticle probes (functionalized with sequences **a** and **b**, respectively, Table 1) that have been designed to recognize a target sequence (**a′b′**, Table 1), which assembles the particle probes into aggregate structures,[27−29] Scheme 1A. This process can be visualized in solution with the naked eye (red to purple color change) or by UV−vis spectroscopy, Figure 1A and B. In the latter case, spectroscopic signatures associated with the particles at 520 or 260 nm, which are sensitive to aggregation, can be used to monitor the hybridization and dehybridization processes. Note that DNA dehybridization without nanoparticles is typically monitored at 260 nm, and the observed melting curves are associated with a transition dipole in the bases that is quenched upon formation of the duplex structure.[30] When the nanoparticles are present and used in a given assay, the DNA concentration is so low (typically 100 aM−60 nM) that there is negligible contribution of the DNA to the monitored optical signal of the solution. Therefore, a key issue in the nanoparticle systems pertains to the use of the term "melting" to describe the dehybridization process. Because of the enormous difference in extinction values associated with the nanoparticle UV−vis signatures as compared with those of the DNA (extinction coefficient: 2.7×10^8 M^{-1} cm^{-1} at λ_{520} for 13 nm particles and $\sim$10^6 M^{-1} cm^{-1} at λ_{260} for 30-mer oligonucleotides), the observed signal may only be sensitive to the latter stages of the aggregate dissociation process (i.e., initial dissociation events involving DNA but not nanoparticles might not affect the observed transition). The data described herein will address this issue.

The second format involves a substrate (typically glass) functionalized with capture strands of DNA (sequence **a**, Table 1), Scheme 1B. These capture strands are used to recognize and hybridize longer target strands (**a′b′**, Table 1) with regions that are complementary to the immobilized capture strands. Nanoparticle probes that are complementary with a second region of the target are used to provide the signal in the assay

(27) Letsinger, R. L.; Mirkin, C. A.; Elghanian, R.; Mucic, R. C.; Storhoff, J. J. *Phosphorus Sulfur* **1999**, *146*, 359.
(28) Reynolds, R. A.; Mirkin, C. A.; Letsinger, R. L. *Pure Appl. Chem.* **2000**, *72*, 229.
(29) Cao, Y.-W.; Jin, R.; Mirkin, C. A. *J. Am. Chem. Soc.* **2001**, *123*, 7961.
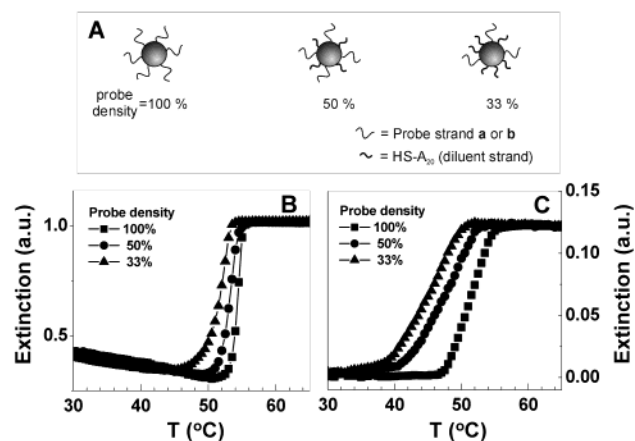(30) Tinoco, I., Jr. *J. Am. Chem. Soc.* **1960**, *82*, 4785.

Figure 2. The effect of probe oligonucleotide density on the Au nanoparticle surface on the melting properties (A) scheme, (B) in solution with aggregates, and (C) in the glass surface system (Au 13 nm particles were used; target concentration = 60 nM, 0.3 M NaCl, pH 7 PBS buffer, tail-to-tail hybridization mode in the aggregrates, see Scheme 2).

(e.g., a color due to absorption or light-scattering of the particles), Figure 1D.[11,31,32]

If one compares the melting properties of these systems, where the DNA sequences are identical in all assays, one concludes that the transitions associated with nanoparticle probes are always substantially sharper than those based on normal analogous molecular fluorophore probes such as Cy-3 and Fluorescein (Scheme 1C). In addition, in general, the systems based upon aggregates of nanoparticle probes exhibit sharper melting profiles than those based on single nanoparticle probe complexation to target. The following experiments are a systematic investigation of some of the potential contributors to the melting properties of these novel materials. Following the experiments, we present our thermodynamic model to account for the experimental observations.

Effect of Probe Oligonucleotide Density on the Au Nanoparticle Surface. In the nanoparticle-based DNA detection systems, the probe oligonucleotides are chemisorbed onto the Au nanoparticle surface and can specifically bind to a single-stranded DNA target and thus report its presence. A high DNA surface density on the nanoparticle is advantageous in terms of particle stabilization, especially at elevated salt concentrations (>0.1 M), which are necessary to effect DNA hybridization. Moreover, the high surface density of the probe DNA could potentially increase the hybridization efficiency (as will be explained later), resulting in cooperativity in the melting process. Therefore, it is important to study the melting of DNA in the context of aggregates and surface particle monolayers as a function of probe oligonucleotide density, Figure 2A.

To adjust the DNA density on the nanoparticle surface while still maintaining adequate particle stability under high salt concentration (0.1−1.0 M NaCl), diluent strands **1** (for probe **a**, Table 1) and **2** (for probe **b**, Table 1) were used to adjust the surface density of the probe oligoncucleotides on the nanoparticle surfaces, Figure 2A. By coadsorbing the diluent strands with the appropriate probe strands onto the Au nanoparticles, one can control the surface density of the probe strands; indeed, in a separate study, the surface density of the probe oligonucle-

otides was found to increase linearly with the mole percent of the probe strand in the deposition solution over a 10−100% concentration range.[33]

Under comparable experimental conditions, the as-prepared nanoparticle probes were hybridized with target to form aggregates, Scheme 1A. The melting analyses show that the T_m is directly proportional to the probe surface density when the nanoparticle and target concentrations are kept constant, Figure 2B. The T_m decreased from 54.4 °C for 100% probe surface density (no dilution) to 52.5 °C when both sets of particles were at 50% probe density, and down to 51.3 °C when both sets of Au particles were at 33% probe density. Also, a slight broadening of the melting transition was observed as the probe density decreased from 100% (fwhm = 2.5 °C) to 33% (fwhm = 3.4 °C).

Interestingly, we also observed qualitatively similar behavior for nanoparticle probes with different surface probe densities that were hybridized to glass substrate surfaces, Scheme 1B and Figure 2C. In these experiments, a single layer of nanoparticles was hybridized to the glass substrate (300 μm diameter beads), and the melting process was monitored in a quartz cuvette by UV−vis spectroscopy. As in the case of the aggregates, the T_m decreased with decreasing probe surface density. Again, the breadth of the melting transition increased slightly as the probe DNA density decreased from 100% (fwhm = 3.2 °C) to 33% (fwhm = 5.0 °C). The T_m values are not comparable with the solution system because these two systems are different in some aspects even when using the same particle probes with the same dilution extent. For example, the effective capture strand concentrations are different. Regardless, the trend involving the probe surface density is valid and shows that the T_m is lowered with decreasing probe surface density, and the melting transition broadens; however, the transition is still significantly sharper than that for unmodified DNA of identical sequence (fwhm = 10 °C).

Effect of Au Nanoparticle Size. The size of the nanoparticle often dictates the types of formats that can be used to detect DNA hybridization events. For example, 13 nm diameter particles are ideal for the spot test (Figure 1C), but larger particles are required for light-scattering formats (30−100 nm diameter), Figure 1D. In this work, Au nanoparticles with average diameters of 13.0 (±1.2), 31 (±3), and 50 nm (±4.5 nm), respectively, were selected (Supporting Infomation). Interestingly, we have discovered that the melting properties of these nanoparticle probes are also highly dependent on the particle size, Figure 3.

In the glass surface system, the melting properties of different sized nanoparticle probes (functionalized with sequence **b**, Table 1) were studied off of glass beads (300 μm diameter) modified with capture strands (sequence **a**, Table 1). Importantly, the melting analyses show that the melting transitions for the 50 nm particles are distinctly sharper than those for the 31 and 13 nm particles, Figure 3A. Such particle size-dependent melting behavior also was observed in the solution aggregate system, Figure 3B. Indeed, in the solution system, the fwhm for the first derivative of the melting transition associated was only 0.5 °C for the 50 nm particles, 1.5 °C for the 31 nm particles,

(31) Taton, T. A.; Lu, G.; Mirkin, C. A. *J. Am. Chem. Soc.* **2001**, *123*, 5164.
(32) Jin, R.; Cao, Y.; Mirkin, C. A.; Kelly, K. L.; Schatz, G. C.; Zheng, J. G. *Science* **2001**, *294*, 1901.

(33) Demers, L. M.; Mirkin, C. A.; Mucic, R. C.; Reynolds, R. A.; Letsinger, R. L.; Elghanian, R.; Viswanadham, G. *Anal. Chem.* **2000**, *72*, 5535.
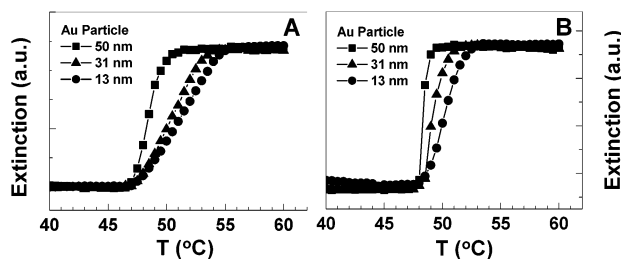
Figure 3. The effect of nanoparticle size on the melting of (A) particle probes off of glass substrates (250−300 μm beads) and (B) particle aggregates in the solution system (head-to-tail hybridization mode in the aggregate, see Scheme 2). The spectral maximum (λ_{max}) was monitored as a function of temperature (λ_{max} = 520, 528, and 540 nm, respectively, for 13, 31, and 50 nm Au particle probes). Extinctions are normalized for ease of comparison.

and 2.5 °C for the 13 nm particles. Note that the variation of the T_m values in these experiments is difficult to evaluate because it depends on the surface DNA coverage,[34] target concentration (see Experimental Section), and local dielectric environment, which are not identical from experiment to experiment.

The physical size and corresponding diffusion properties of the particles are not likely the major contributors to the sharp melting profiles observed for these nanoparticle probes. Indeed, others have shown that large dendrimers[35] and even micrometer-scale polymer particles exhibit relatively broad melting profiles.[28] The Au nanoparticles studied herein have been heavily functionalized with oligonucleotides ($\sim$10^{13} strands/cm^2), which substantially affect their melting properties by creating multiple equivalent sites for cooperative dehybridization. On the other hand, micrometer-scale latex particles typically have relatively low surface coverages of probe DNA ($<$10^{11} strand/cm^2),[28] which apparently does not allow for comparable cooperative behavior. Indeed, theoretical calculations suggest that the cooperative effect occurs over a short range, that is, duplex-to-duplex spacings $<$5 nm.[36]

Effect of Salt Concentration. To determine the effect of increasing salt concentration on the melting properties of DNA-linked nanoparticle aggregates, we studied melting behavior as a function of NaCl concentration, Figure 4. The melting analyses show that salt concentration substantially affects the T_m of the nanoparticle aggregates. As the salt concentration was increased from 0.05 to 1.0 M while keeping the nanoparticle and target concentration constant, the T_m increased from 41 to 61.5 °C, with a slope of dT_m/d log[Na$^+$] = 15.8, Figure 4A,B. Normal DNA of identical sequence exhibits a similar salt concentration dependence but with lower absolute T_m values, Figure 4B. This is consistent with the conclusion that the increased dielectric created by the nanoparticle probes stabilizes the duplex DNA interconnects. Note that this effect is more substantial than it appears in Figure 4B, because the concentrations of the nanoparticles (1.5 nM for each particle probe) and target DNA (60 nM) are substantially lower than those of the oligonucle-
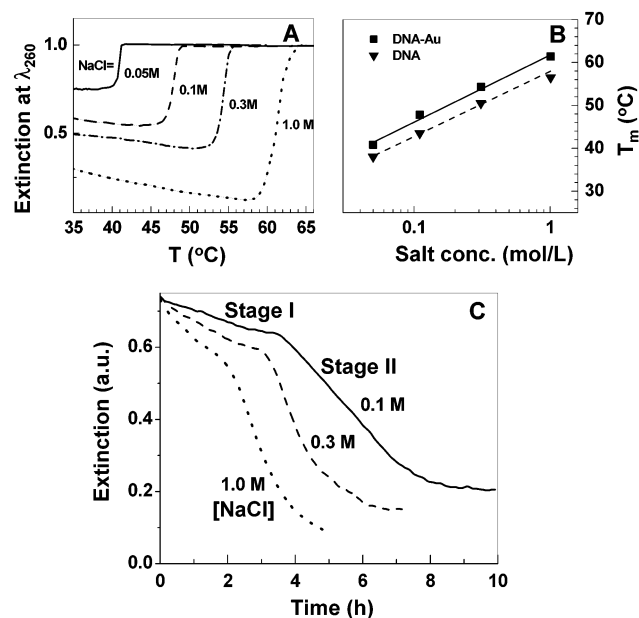
(34) The oligonucleotide surface coverage on the nanoparticle was determined to be ~90, 160, and 250 single strands per 13, 31, and 50 nm diameter Au particles, respectively.
(35) Shchepinov, M. S.; Mir, K. U.; Elder, J. K.; Frank-Kamenetskii, M. D.; Southern, E. M. *Nucleic Acids Res.* **1999**, *27*, 3035.
(36) Long, H.; Schatz, G. C. *Mat. Res. Soc. Proc.* **2002**, *735*, C01.
(37) Storhoff, J. J.; Lazarides, A. A.; Mucic, R. C.; Mirkin, C. A.; Letsinger, R. L.; Schatz, G. C. *J. Am. Chem. Soc.* **2000**, *122*, 4640.

Figure 4. (A) The effect of salt concentration on the melting of nanoparticle aggregates in the solution system. (B) The plot of T_m as a function of salt concentration in the presence of oligonucleotide-functionalized nanoparticle probes (solid line) or ordinary oligonucleotides (dashed line). (C) The effect of salt concentration on the hybridization kinetics of nanoparticle probes with target in the solution system. The kinetic curves were monitored at 520 nm, and the solution was not stirred during the experiment (Au 13 nm particles, target concentration = 60 nM, pH 7 PBS buffer, tail-to-tail hybridization mode in the aggregates, see Scheme 2).

otides in the pure DNA system (target $\sim$1 μM, sequence **a**:**b**:**a′b′** = 1:1:1).

A second effect of increasing salt concentration is that larger aggregates form as evidenced by larger extinction changes during melting (Figure 4A), which has been further confirmed by light-scattering measurements.[37] This is likely due to a screening effect of the salt, which minimizes electrostatic repulsion between the oligonucleotide-modified particles, allowing more hybridization events to take place, leading to more linked particles and hence larger damping of the surface plasmon absorption of Au nanoparticles. This screening effect is also reflected in an experiment designed to study the hybridization rates as a function of salt concentration, Figure 4C. In such experiments, two sets of nanoparticle probes (total concentration = 3 nM, ratio = 1:1) functionalized with sequences **a** and **b**, respectively (Table 1), and target DNA **a′b′** (60 nM) were dispersed in PBS buffer (10 mM phosphate, pH 7) with salt concentrations of 0.1, 0.3, and 1.0 M, respectively. The hybridization rate was studied by monitoring the extinction of the surface plasmon resonance at 520 nm for 13 nm Au particles as a function of time. As the DNA hybridization proceeds, the signal at 520 nm decreases, indicating aggregation of the Au nanoparticles, Figure 4C. One can clearly see that the hybridization rate is markedly dependent on and directly proportional to increasing salt concentration (stage I, Figure 4C). As the nanoparticle aggregates grow and reach a critical undetermined size, they precipitate from solution (stage II, Figure 4C), thus exhibiting a transition in the 520 nm extinction profile as a function of time. These data clearly show that electrostatic interactions between nanoparticles, which can be tailored by adjusting the salt concentration, play an important role in their hybridization and dehybridization behaviors.
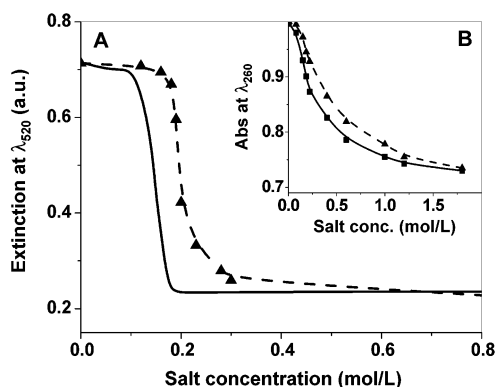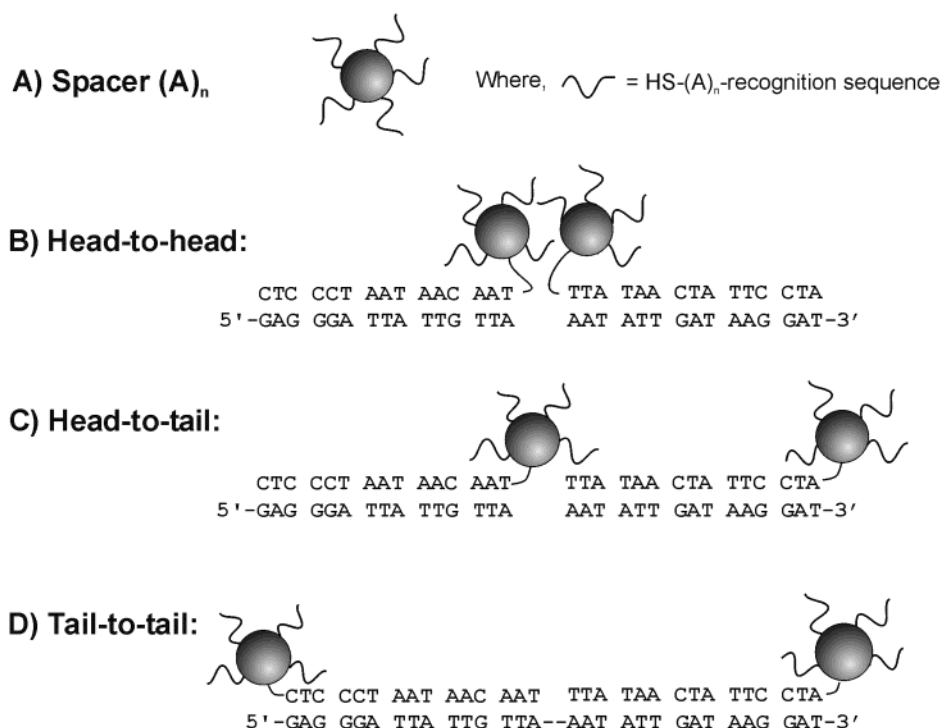
Scheme 2

Figure 5. Salt-induced melting at a fixed temperature of 47 °C for (A) DNA-nanoparticle aggregates and (B) plain DNA. The solid curve corresponds to the perfectly complementary target (**a′b′**, Table 1), and the dashed line correponds to the single base mismatched target (5′-GAG GGA TTA TTG TTA AAT ATT G<u>T</u>T AAG GAT-3′).

Interestingly, once the salt concentration is decreased to less than 0.05 M, the Au nanoparticle probes (total 3 nM with a 1:1 ratio) do not hybridize at room temperature in the presence of target (60 nM), as evidenced by the absence of surface plasmon resonance damping and redshifting. In contrast, complementary oligonucleotides (in the absence of nanoparticles) having the same sequence as those on the particles will hybridize at 0.05 M NaCl or less. These observations enable one to control the DNA-nanoparticle hybridization/dehybridization processes by adjusting salt concentration at or above room temperature, Figure 5A. Significantly, the range of salt concentration over which dehybridization takes place is very narrow (0.1 M) and can be used to readily discriminate between perfectly complementary targets and single-base mismatched strands, Figure 5A. The analogous experiments done with oligonucleotides in solution that have the same sequence as those attached to particles show very broad melting behavior, Figure 5B. These unusually narrow

salt-induced melting transitions involving nanoparticles are important because they can be used to develop high selectivity detection assays and potentially eliminate the need for thermal stringency.[38]

Effect of Interparticle Distance. As nanoparticles are linked together via DNA hybridization, electromagnetic coupling between the nanoparticles results in significant damping of their surface plasmon resonances and a distinct color change from red to purple, which enables their use in colorimetric detection. Interparticle distance also influences van der Waals and electrostatic forces between the particles, affecting duplex DNA stability and hybridization/dehybridization properties. To study the effect of interparticle distance on the melting properties of the nanoparticle aggregates, we have utilized different length oligonucleotide spacers, $(A)_n$, or have simply changed the nanoparticle position relative to the oligonucleotide target, Scheme 2.

In the first approach, we introduced spacers $(A)_n$ of various lengths ($n = 0, 10, 20, 30$) between the thiol functionality and the recognition sequence, Scheme 2A. Under comparable experimental conditions, the melting analyses show that the T_m increases with the length of spacer (or the interparticle distance) from 48.5 °C (no spacer) to 58.6 °C (A_{30} spacers), Figure 6A. Moreover, the T_m shows an excellent linear relationship with the length of the $(A)_n$ spacer, T_m (°C) = 48.5 + 0.327*n, where n is the the number of A spacers, Figure 6C (solid line).

The second approach to adjust the interparticle distance is to place the nanoparticle at different positions of the probe oligonucleotide (either 3′ or 5′ position), which can be achieved by functionalizing the nanoparticle with either 3′ or 5′ thiol-capped oligonucleotides, Scheme 2B−D. The melting analyses show that the T_m is very sensitive to the relative position

(38) Park, S.-J.; Taton, T. A.; Mirkin, C. A. *Science* **2002**, *295*, 1503.
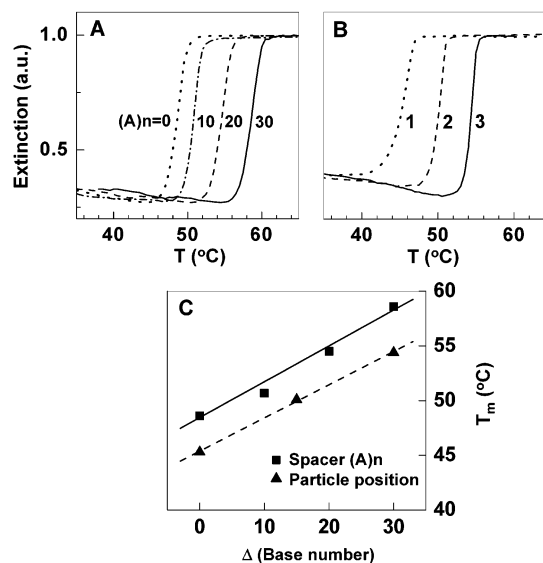
Figure 6. The effect of interparticle distance on the melting properties of nanoparticle aggregates, (A) the length of the poly (A)$_n$ spacer (tail-to-tail hybridization mode), (B) hybridization modes of particles: **1**, head-to-head; **2**, head-to-tail; **3**, tail-to-tail (see Scheme 2). (C) The plots of T_m as a function of changing spacer base number (solid line) and particle probe position (dash line) as a function of base separation (see Scheme 3). Au 13 nm particles were used; target concentration = 60 nM, 0.3 M NaCl PBS buffer.

Figure 7. (A) Circular dichroism (CD) spectrum of hybridized DNA without nanoparticles (0.3 M NaCl PBS, target concentration = 1 μM, sequence **a:b:a′b′** = 1:1:1, see Table 1). (B) The melting curve of DNA without nanoparticles monitored by CD at 248 nm. (C) CD spectrum of DNA-linked nanoparticle aggregates (13 nm Au particles, target concentration = 60 nM, 0.3 M PBS buffer, head-to-tail hybridization mode of particles in aggregrates). (D) The melting curve of particle aggregates monitored by CD at 248 nm.

of particles and that T_m increases with interparticle distance, Figure 6B. Interestingly, the slope of the T_m versus interparticle base numbers is 0.303 °C/base, Figure 6C (dashed line), which is very close to the slope observed in the first approach. This similarity implies that the intrinsic interactions between particles, which affect the melting properties, are related.

The large T_m discrepancy (9−10 °C) in both approaches cannot be explained simply by increased hybridization efficiency (more duplex DNA links) for the structures with larger interparticle distances. Indeed, one can vary the hybridization efficiency by controlling the amount of target available for nanoparticle hybridization over a 10^{-10}−10^{-6} M range, and only a 2.5 °C T_m variation per order of magnitude of target concentration is observed. Thus, even a 100 times difference in the hybridization efficiency would only lead to a T_m difference of 5 °C. Note that there are nearly 90 probe strands on a single 13 nm Au particle; thus, the maximum change of hybridization efficiency is ~100 times. The large T_m differences in the interparticle distance dependence studies are also not due to differences in the aggregate size as evidenced by both the light-scattering and the TEM measurements. Thermal annealing of any of these aggregates, which is known to facilitate aggregate growth,[37] does not change the T_m by more than 1 °C. Therefore, we conclude that electrostatic interactions (particle−particle repulsion), which would be expected to be sensitive to the interparticle distance, are the dominant factors which affect the T_m in these studies.

Mechanistic Studies of DNA Melting in the Presence of Nanoparticles. Before we discuss the melting process for the DNA-nanoparticle system, it is necessary to briefly review the accepted melting mechanism of ordinary DNA. When a solution of duplex DNA is heated above a characteristic temperature, the helical duplex structure undergoes collapse, accompanied by the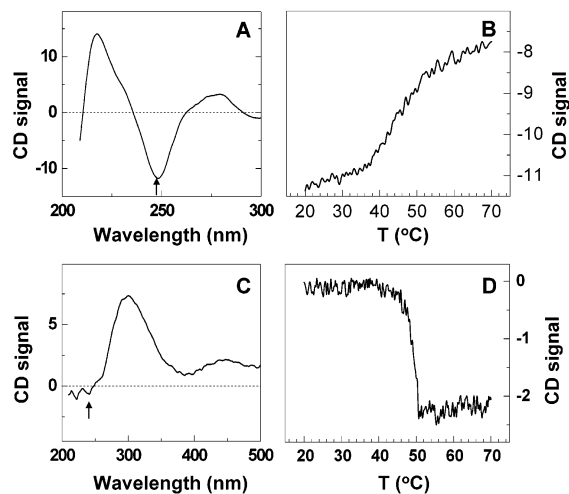 separation of the two complementary strands and a concomitant increase in absorption at ~260 nm.[39] A "cooperative effect" in the duplex melting process is often observed: more mobile AT-rich internal regions melt first; these melted regions destabilize the neighboring helical structure, and hence a concerted melting of the entire helical structure at the T_m takes place. Such cooperativity also explains the observation that within the coherent length of DNA, the longer the DNA duplex, the sharper the melting transition.[40]

To investigate the importance of DNA dehybridization during the early stages of aggregate melting, which might not be reflected in the UV−vis spectroscopy,[10,37,41] we utilized circular dichroism (CD) and fluorescence spectroscopies as tools for monitoring the melting process because they can be used to monitor the signal from DNA (or fluorophore-functionalized DNA) within the aggregate rather than from the nanoparticles.

The CD spectroscopy reveals that the DNA duplexes in these studies are in a B-form conformation, as evidenced by a negative band at 248 nm and a positive band at 280 nm,[42] Figure 7A. The CD melting curve for ordinary duplex DNA, monitored at 248 nm versus temperature, is similar in breadth (fwhm = 11 °C) to the melting curve measured by UV−vis spectroscopy (fwhm = 10 °C), Figure 7B. In the solution aggregate system (hybridized form), the CD spectrum shows that the positive band red-shifts from 280 to 300 nm and that the negative band at 248 nm broadens and becomes nondescript, Figure 7C. The CD melting curve for the aggregate, monitored at 248 nm, shows a sharp melting transition (fwhm = 3 °C) with no premelting behavior prior to the main melting transition, Figure 7D, indicating a cooperative melting of the duplex DNA interconnects that make up the aggregate.

(39) Voet, D.; Gratzer, W. B.; Cox, R. A.; Doty, P. *Biopolymer* **1963**, *1*, 205.
(40) (a) Porschke, D. *Biopolymers* **1971**, *10*, 1989. (b) Crothers, D. M. *Biopolymers* **1968**, *6*, 1391.
(41) Li, Z.; Jin, R.; Mirkin, C. A.; Letsinger, R. L. *Nucleic Acids Res.* **2002**, *30*, 1558.
(42) (a) Sprecher, C. A.; Johnson, W. C., Jr. *Biopolymers* **1982**, *21*, 321. (b) Davis, T. M.; McFail-Isom, L.; Keane, E.; Williams, L. D. *Biochemistry* **1998**, *37*, 6975.

Scheme 3
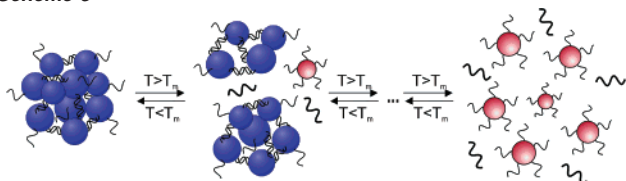
We also carried out a melting analysis using fluorescence spectroscopy. In such experiments, fluorophore Cy3-capped targets were used to replace the normal targets to form nanoparticle aggregates. Prior to DNA melting, the fluorescent signal from Cy3-capped targets is significantly quenched by the Au nanoparticles due to energy transfer from the excited fluorophores to the nanoparticles; however, after DNA melting, the target is released, and the fluorescence signal is recovered, providing a way of monitoring the melting process. A sharp melting transition, similar to the temperature-dependent UV−vis spectroscopy and CD spectroscopy measurements, was observed (fwhm = 3 °C, melting curve not shown).

Taken together, all of these results show that the duplex DNA interconnects, within the nanoparticle aggregate, melt in a highly cooperative manner. An additional clue concerning the cooperative melting process is provided by studies of DNA melting for the surface system as a function of the number of surface layers. It has been shown that the melting transition gradually sharpens as an aggregate structure is built in a layer-by-layer fashion on a glass surface.[11]

Thermodynamic Melting Model

The Model. Simple thermodynamic analysis has been widely used in the study of melting curves for oligomer strands, from monomolecular (e.g., hairpins) and bimolecular (e.g., duplexes)[43,44] to high-order nucleic acid structures, such as DNA junction structures[45] and DNA tetraplexes.[46] The melting of DNA-linked nanoparticle assemblies differs from these other systems in many ways. Key features of the DNA-nanoparticle system that control the melting behavior are (1) there are multiple DNA links between the particles, and (2) these DNA strands experience high local dielectric due to the high loading of DNA on the particles.

Assuming that there are many nanoparticles in the aggregate and that each pair of particles are linked by many DNA duplexes, we found that the melting will involve a series of steps, Scheme 3. Here we imagine that in each step the aggregate releases a target oligonucleotide Q, along with its complement of salt ions S.[47] The aggregate may also partially disintegrate in this process, but to keep things simple, we will collect all of the nanoparticles originally in the aggregate into a group, whose concentration is denoted as D_i. Here the subscript i indicates the number of targets per nanoparticle that are still attached to the group. With these definitions, the melting process can be represented using the equations:

(43) Marky, L. A.; Breslauer, K. J. *Biopolymers* **1987**, *26*, 1601.
(44) Breslauer, K. J. *Methods Enzymol.* **1995**, *259*, 221.
(45) Marky, L. A.; Kallenbach, N. R.; McDonough, K. A.; Seeman, N. C.; Breslauer, K. J. *Biopolymers* **1987**, *26*, 1621.
(46) (a) Jin, R.; Breslauer, K. J.; Jones, R. A.; Gaffney, B. L. *Science* **1990**, *250*, 543.(b) Jin, R.; Gaffney, B. L.; Wang, C.; Jones, R. A.; Breslauer, K. J. *Proc. Natl. Acad. Sci. U.S.A.* **1992**, *89*, 8832.
(47) Particles linked directly through surface bound DNA, the two-strand system, still show cooperative melting, as the counterions are still released when melting occurs (as the fraction of condensed counterions is lower in single-stranded DNA than it is in double-stranded DNA).

$$D_N = D_{N-1} + Q + nS;$$
$$\cdots \quad \cdots$$
$$D_2 = D_1 + Q + nS;$$
$$D_1 = D_0 + Q + nS. \tag{1}$$

where in each step we assume that n free salt ions are released per target strand. The number N is the total number of targets in the aggregate per nanoparticle, and D_0 refers to the completely dispersed state of the aggregate that occurs when all of the targets have melted.

As a measure of the progress of melting, we calculate the fraction of total aggregate that is in state D_0, that is

$$f = \frac{D_0}{D_T} = \frac{D_0}{\sum_i D_i} = \frac{1}{1 + \frac{1}{K}} \tag{2}$$

where D_T is the total concentration of aggregate. The overall equilibrium constant K is related to the equilibrium constants K_i associated with the steps in (1) via

$$\frac{1}{K} = \frac{Q \cdot S^n}{K_1}\left(1 + \frac{Q \cdot S^n}{K_2} + \frac{Q^2 \cdot S^{2n}}{K_2 K_3} + \cdots + \frac{Q^{N-1} \cdot S^{n(N-1)}}{K_2 K_3 \cdots K_N}\right) \approx$$
$$\frac{Q^N \cdot S^{nN}}{K_1 K_2 K_3 \cdots K_N} \tag{3}$$

Here the last term is dominant if the melting temperature for each step in eq 1 *decreases* as melting takes place. This is the key assumption that introduces cooperativity into the mechanism, and it is based on the idea that the local salt concentration in the vicinity of the aggregate gradually decreases as melting takes place. Such a drop in ion concentration is known experimentally to decrease the melting temperature (vide supra), and in a future publication where the thermodynamic model is described in greater detail,[36] we use atomistic simulations to show that DNA aggregates experience higher local salt concentration (and a higher fraction of condensed counterions) than in unaggregated DNA for loadings that are likely to occur in the Au nanoparticle aggregates, that is, DNA separations of less than 5 nm.

A useful expression for the melting curve is obtained by using the van't Hoff formula for the equilibrium constant K_i:

$$K_i = QS^n \exp\left(-\frac{\Delta H_i}{R}\left(\frac{1}{T} - \frac{1}{T_{m,i}}\right)\right) \tag{4}$$

where $T_{m,i}$ refers to the Q- and S-dependent melting temperature of step i (defined such that $K_i/QS^n = 1$ when $T = T_{m,i}$). Substitution of eq 4 into eq 3, and using eq 2, we obtain the following expression for the melting curve:

$$f = \frac{1}{1 + \exp\left(\frac{\Delta H_{tot}}{R}\left(\frac{1}{T} - \frac{1}{T_m}\right)\right)} \tag{5}$$

where

$$\Delta H_{tot} = \sum_i \Delta H_i \tag{6}$$

and

$$T_m = \frac{\Delta H_{tot}}{\sum_i \dfrac{\Delta H_i}{T_{m,i}}} \tag{7}$$

These expressions indicate that the breadth of the melting curve is determined by the total enthalpy of melting ΔH_{tot}, while the overall melting temperature T_m (defined as the temperature where the derivative of f with respect to T shows a maximum) is a weighted average of the individual melting temperatures. Note that there is an exponential sensitivity of the melting curve on ΔH_{tot} so that even $N = 2$ (i.e., two linkers per pair of particles) will produce a significant narrowing in the melting breadth. If the target or salt concentration is changed, the temperatures $T_{m,i}$ of the individual melting steps are changed, leading to a change in the overall melting temperature T_m, but not in the enthalpy or width. Thus, the target or salt concentration influences the melting entropy, while the number of linkers influences the melting enthalpy.

This analysis shows that by fitting f to the experimental data, one can determine ΔH_{tot} and T_m. ΔH_{tot} can be obtained from the derivative of eq 5 evaluated at $T = T_m$:

$$\Delta H_{tot} = 4R \cdot T_m^2 \cdot \left[\frac{df}{dT}\right]_{T_m} \tag{8}$$

Here df/dT at T_m measures the sharpness of the melting because it is inversely proportional to the fwhm.

To provide further information concerning parameters in the cooperative melting model, we need to examine the dependence of the melting temperature on target and salt concentrations. If we evaluate eq 3 at the melting temperature for unit target and salt concentration (i.e., $T_m(S = 1, Q = 1)$), and then substitute eq 4, we find:

$$nN \ln S + N \ln Q = -\frac{\Delta H_{tot}}{R}\left(\frac{1}{T_m(S,Q)} - \frac{1}{T_m(S = 1, Q = 1)}\right) \tag{9}$$

Differentiating eq 9 with respect to the salt concentration, we find

$$\frac{dT_m}{d \ln S} = \frac{nNRT_m^2}{\Delta H_{tot}} \tag{10}$$

which indicates that $d(1/T_m)/d \ln S$ does not depend on the melting temperature. A similar derivation gives the following expression for the dependence of melting temperature on target concentration:

$$\frac{dT_m}{d \ln Q} = \frac{NRT_m^2}{\Delta H_{tot}} \tag{11}$$

This analysis shows that once T_m and ΔH_{tot} are determined by fitting the experimental melting curve, one can determine N, the number of targets that melt cooperatively, using eq 11. In addition, the ratio of the two slopes [eqs 10 and 11] gives n, the number of released counterions per melting step.

Extensions and Limitations of the Model. Although we have used the species D_0 to monitor melting in this derivation,
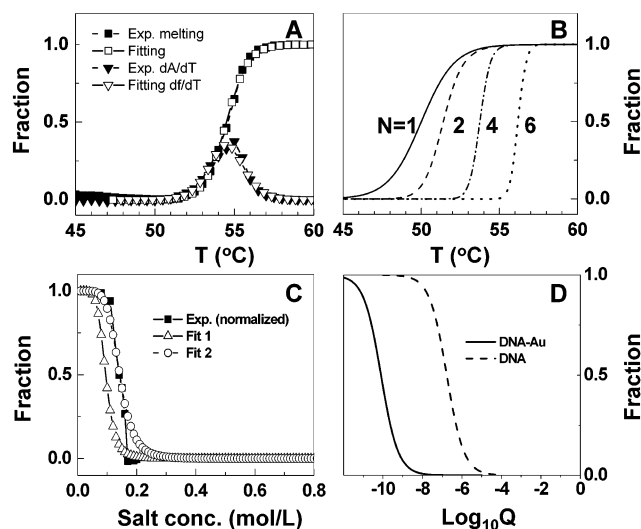
Figure 8. (A) Fit of cooperative model to experimental data for the DNA-linked 13 nm Au particle results. (B) Effect of the number of DNA linkers on the melting curve. Here we use the cooperative model with $\Delta H_i = 200$ kcal/mol and $T_{m,i} = 50\,°C + (i - 1)2.5$. (C) Salt-induced melting curves (fraction melted vs salt concentration) for the DNA/nanoparticle aggregates. Fit **1** shows the predicted result from the cooperative model ($\Delta H_i = 198$ kcal/mol, $n = 6.2$); fit **2** shows a slight adjustment to the cooperative model that provides more quantitative fits to the data ($\Delta H_i = 182$ kcal/mol, $n = 6.2$). (D) Target-induced melting for DNA-linked nanoparticle aggregate and plain DNA in solution.

one can use other variables such as the target concentration Q. We find that the melting curve associated with Q shows narrow melting very similar to that for D_0. This is consistent with the experimental results described earlier.

To keep the model as simple as possible, we have left out details of the aggregate size or structure. Of course, if size or structure influences the parameters of the model, that is, N, ΔH_i, or $T_{m,i}$, then the model can be used to interpret this effect. For example, it is likely that the effective N value is larger for bulk aggregates than for a monolayer of nanoparticles that are hybridized to surfaces. This should lead to sharper melting for the bulk aggregates, as observed in Figure 2. This argument also applies to the dependence of the melting behavior on nanoparticle size, as will be described in the next section.

One limitation of the model is that the only role of the nanoparticles is to provide DNA binding sites so that there can be a high surface density of DNA and multiple links between nanoparticles. This means that electrostatic interactions between charged nanoparticles, or between the nanoparticles and DNA, are not taken into account. Some consequences of this will be discussed in the next section.

Model Results and Discussion

Fitting the Experimental Data. For a 30 bp DNA-linked 13 nm Au particle aggregate, Figure 8A shows an excellent fit between the results from eq 5 and those from experimental melting measurements. The fit yields $\Delta H_{tot} = 317$ kcal/mol and $T_m = 54.5\,°C$. These values, combined with the target concentration-derivative $dT_m/d \log Q = 2.55$, give $N = 1.6$ using eq 11. This indicates that the number of cooperatively melting DNA strands is roughly twice the number of nanoparticles. Note that even with 1.6 linkers per particle, there are still multiple closely spaced duplex linkages for each nanoparticle in the aggregate.

Table 2. Melting Temperatures and Enthalpies for Different Sized Nanoparticles in the Solution Aggregate System

particle diameter (nm)	T_m (°C)	ΔH_{tot} (kcal/mol)
13	50	275.8
31	49	473.8
50	48.5	706.8

As a consistency check for this estimate of N, we have used the Hyther thermodynamics model[48] to determine ΔH_i for individual melting steps. Here we make the assumptions that all of the enthalpies ΔH_i are the same and that these enthalpies are the same as the enthalpy of plain DNA. Using the Hyther model, we calculated the solution enthalpy to be 221.8 kcal/mol for the 30 bp duplex being considered. From this, one can calculate the ratio $\Delta H_{tot}/\Delta H_i = 317/221.8 = 1.4$, which is similar to the N value estimated by the value of $dT_m/d \log Q$ given above.

Another check on the validity of our cooperative melting model may be inferred from the variation of T_m with respect to salt concentration. The slope $dT_m/d \log S$ is 15.8 from the measurements, which means that if S changes by a factor of 2 (which would be representative of the possible change in local salt concentration when the aggregate melts), T_m decreases by 5 °C. This is significantly larger than the width of the melting curve, which is what is needed for the right-hand term of eq 3, that is, the cooperative limit, to be valid.

The ratio of the slope of T_m with respect to S to the slope of T_m with respect to Q provides an estimate of the number of free counterions per target. The measured slopes yield a value of 6.2 for this ratio, which is similar to that found in solution measurements (we obtained a value of 5.1 for plain DNA with the same sequence). This ratio indicates that roughly 20% of the counterions associated with the 30 bp target are free, which is a number that can be compared with results of atomistic simulations.[36]

Record and co-workers have studied the relation between the magnitude of the salt dependence and the degree of thermodynamic association of ions with the helix and coil forms.[49−51] On the basis of their formulation, we can write the following equation to describe the salt effect for our system:

$$nN = -\frac{d \ln K}{d \ln S} = \frac{\Delta H_{tot}}{RT_m^2}\frac{dT_m}{d \ln S} = 2N^*\Delta\Gamma_N \qquad (12)$$

where N^* is the number of phosphates in each duplex (here 58 for 30 bp DNA), and $\Delta\Gamma$ is the preferential interaction coefficient per phosphate. Because the total number of counterions released from melting is about 10 ($n \times N = 6.2 \times 1.6$), we find $\Delta\Gamma = 10.0/(29 \times 2 \times 2) = 0.0862$, which is close to values obtained for many oligonucleotide systems.[49−51]

Effect of Nanoparticle Size. For the experiments involving larger nanoparticles, the melting curves are sharper, and fits to the cooperative model yield larger values of ΔH_{tot}, Table 2.

The interpretation of these results is that the number of linkers increases (roughly doubling and tripling) as the nanoparticle size increases. Figure 8B shows how the melting curves sharpen as the number of linkers between the nanoparticles increases. Note that in the experimental data, Figure 3B, the melting temperature drops slightly as the particle diameter increases because the target concentration was chosen to be smaller for the larger particles. Although the oligonucleotide surface density decreases with increasing Au nanoparticle size,[34] which should result in broadening of the melting transition, the number of linkers per particle-pair exceeds this effect, and hence sharper melting occurs as the particle size is increased.

Salt-Induced Melting. The experiments show that melting can be induced by decreasing the salt concentration at constant temperature. This is described in the cooperative melting model, and, indeed, with the parameters determined by fitting the thermal melting curve and the slope $dT_m/d \ln S$ and $dT_m/d \ln Q$, one can predict the salt-induced melting curve without any additional parametrization. Figure 8C shows the results of this calculation (fit **1** curve) for a fixed temperature of 47 °C and using the enthalpy and melting temperature parameters derived from the $S = 0.3$ M, $Q = 60$ nM thermal melting fits. The plot shows that the salt-induced melting transition is predicted to occur at a salt concentration of about 0.10 M (for 60 nM target concentration), while the experimental value is 0.15 M. The close match between theory and experiment, both for the melting salt concentration and for the width of the salt-induced melting curve, shows that the model correctly describes the interplay between temperature and salt effects. Note that the sharpness of the bottom of the measured melting curve is due to annealing of kinetic structures and does not represent a discrepancy between the thermodynamic model and experiment. The additional curve in Figure 8C (fit **2** curve) is to show that decreasing ΔH_{tot} by about 5% (within the uncertainty of the fit to experiment) leads to a better fit to the data.

The cooperative model also indicates that melting can be induced by lowering the target concentration, Figure 8D. The target concentration corresponding to the melting transition of DNA-linked aggregates at 47 °C and for salt concentration (S) $= 0.3$ M is $\sim 10^{-10}$ M, while the corresponding concentration for plain DNA is $\sim 10^{-7}$ M at 47 °C and $S = 0.3$ M . The figure also suggests that only a few percent of surface DNA strands lead to aggregates in the DNA-nanoparticle system for 10^{-12} M concentration of target. This is one of the reasons why the DNA spot test, based on nanoparticle aggregates, has a sensitivity limit in this range.[10]

Effect of Probe DNA Density. When the surface probe strands are diluted with noncomplementary strands (HS-A$_{20}$), the measurements show that melting temperature decreases and the transition broadens, Figure 2A and B. The cooperative melting model provides a qualitative way to understand these results. For such a system, we assume that there are still multiple dissociation steps, but some of the steps are associated with the melting (or "unfolding") of noncomplementary DNA rather than complementary DNA.[52] This means that the effect of dilution is to decrease ΔH_{tot} and T_m, while still preserving the functional form of the melting curve from the cooperative model. Table 3 gives the enthalpies and melting temperatures for

(48) (a) SantaLucia, J., Jr. *Proc. Natl. Acad. Sci. U.S.A.* **1998**, *95*, 1460. (b) Peyret, N.; Seneviratne, P. A.; Allawi, H. T.; SantaLucia, J., Jr.; *Biochemistry* **1999**, *38*, 3468.
(49) Anderson, C. F.; Record, M. T., Jr. *Annu. Rev. Phys. Chem.* **1982**, *33*, 191.
(50) Olmsted, M. C.; Anderson, C. F.; Record, M. T., Jr. *Biopolymers* **1991**, *31*, 1593.
(51) Bond, J. P.; Anderson, C. F.; Record, M. T., Jr. *Biophys. J.* **1994**, *67*, 825.

(52) Holbrook, J. A.; Capp, M. W.; Saecker, R. M.; Record, M. T., Jr. *Biochemistry* **1999**, *38*, 8409.

Table 3. Melting Temperatures and Enthalpies for Different Surface Densities of Probe Oligonucleotides on the Nanoparticles in the Solution System

surface density of probe oligonucleotides	T_m (°C)	ΔH_{tot} (kcal/mol)
33%	51.3	326.0
50%	52.5	415.0
100%	54.5	503.9

different probe DNA densities that we have obtained by fitting the observations, Figure 2A, to the cooperative model. If we make the simplified assumption that all of the ΔH_i's for the undiluted case are the same, we have $N\Delta H_i = \Delta H_{tot} = 504$ kcal/mol for 100% probe density. We now take the diluted enthalpy to satisfy $\Delta H_{tot} = f_c N\Delta H_i + \Delta H_n$, where f_c is the fraction of complementary DNA, and ΔH_n is the total non-complementary enthalpy. If we substitute the $f_c = 0.33$ and $f_c = 0.5$ values from Table 3, we find that $\Delta H_n = 160$ kcal/mol for $f_c = 0.33$ and 163 kcal/mol for $f_c = 0.5$. These results show that the noncomplementary enthalpy is smaller than the complementary enthalpy. Note, however, that in agreement with studies of plain DNA,[44] the noncomplementary enthalpy is still quite large. Presumably, this enthalpy is made up of contributions from several noncomplementary contacts.

Effect of Interparticle Distance. The cooperative model may also be used to interpret the effect of adding poly A segments at each end of the complementary duplex in Figure 6A. These spacer oligonucleotides will increase the local salt concentration surrounding the duplexes, and they will also stabilize the frayed ends of the duplex portion of the linkers. However, the spacer oligonucleotides should not change the number of linkers, so the melting width should not be affected. Thus, the model predicts that the melting temperature but not the width should increase, as seen in Figure 6A.

The results in Figure 6B are more difficult to interpret in view of our model, as these involve structural changes in the aggregates and nanoparticle interactions that are not contained in the thermodynamic model. In particular, we expect that changing the locations of the nanoparticles within the aggregates will influence both counterion concentration (because the nanoparticles are charged) and hybridization efficiency. One can easily imagine how both factors would favor the tail-to-tail configuration, but providing a quantitative description of this effect will require a more explicit description of the aggregate structures than is currently contained in the model.

Conclusions

This work provides a number of important observations and conclusions. First, the "melting transitions" observed for aggregates or individual particle layers hybridized to surfaces are indeed measurements of the entire cooperative melting processes, rather than spectroscopic glimpses of the last stage of the melting process. Second, the melting properties of DNA-linked nanoparticle aggregates are affected by a number of factors, including DNA surface density, nanoparticle size, interparticle distance, and salt concentration. As with native DNA, the T_m of these DNA-linked nanoparticle structures increases with increasing salt concentration. However, changes in salt concentration do not substantially affect the sharpness of the transition. The sharp salt-induced melting of the DNA-nanoparticle system, which is not observed in unmodified

oligonucleotides of the same sequence, allows one to readily discriminate between perfectly complementary targets and single-base mismatched strands and, thus, to develop high selectivity detection assays and potentially eliminate the need for thermal stringency. There also is a strong dependence of T_m on interparticle distance; in general, T_m increases with increasing interparticle distance for the DNA-linked nanoparticle aggregates due to less electrostatic/steric repulsion and hence stabilization of the duplex interconnects. These data are consistent with the conclusion that longer DNA links provide stronger electrostatic stabilization. Increasing probe oligonucleotide density on the nanoparticle surfaces leads to modest increases in T_m and sharper melting profiles. Significantly, the sharpness of the melting profile is highly dependent on nanoparticle size, with 50 nm Au particles exhibiting a melting transition of only a single degree (fwhm = 0.5 °C). Because the sharpness of the melting transition directly correlates with the selectivity of an assay based upon it, this observation points toward a way of greatly improving the selectivity of DNA detection systems based upon nanoparticles. Third, we have found that a cooperative melting model provides a useful way to interpret the DNA/nanoparticle melting results, suggesting that it is the multiple links between the nanoparticles together with the dependence of melting temperature on local salt concentration that are responsible for the narrow melting transitions. Among the successful features of the thermodynamic model are the following: (1) The sigmoidal functional form of the melting curves. By fitting experimental melting data, we determined a melting enthalpy ΔH_{tot} that is larger than the plain DNA result by an amount which reflects the number of links between pairs of particles. (2) Variation of the T_m with respect to target concentration, $dT_m/d \ln Q$. This slope can be used to determine a value for N, the ratio of linkers to nanoparticles, that is roughly 2 for the 13 nm particles. (3) Variation of the T_m with respect to salt concentration, $dT_m/d \ln S$, and the accurate description of salt-induced melting. The slopes show that the number of free ions per target is about six, which is similar to that found in plain DNA studies. The influence of salt on the melting of DNA comes from the fact that DNA is a highly charged molecule, and the local salt concentration near DNA changes after the dissociation of double helices into single strands. (4) Qualitative information about the effect of dilution of the complementary oligonucleotides with noncomplementary oligonucleotides on the melting curves. Here we find that noncomplementary interactions have a lower enthalpy but still make important contributions to the melting curves. Extensions of the model to include for explicit charges on the nanoparticles will be needed to describe the destabilization of the DNA links that occurs when the nanoparticles are forced to be close together. Finally, although Au nanoparticles are used throughout the studies, the above results are also valid with respect to other nanoparticle compositions, such as semiconductor CdSe/ZnS,[53] coreshell Ag/Au,[29] and alloy Ag/Au nanoparticles,[54] but only if they are heavily functionalized with oligonucleotides.

Experimental Section

Synthesis of DNA. The base sequences of the probe (15-mer) and target DNA (30-mer) are adapted from the 141-bp anthrax protective

(53) Mitchell, G. P.; Mirkin, C. A.; Letsinger, R. L. *J. Am. Chem. Soc.* **1999**, *121*, 8122.
(54) Li, Z.; Mirkin, C. A., unpublished work.

antigen gene. All of the oligonucleotides were synthesized on a 1 μmol scale using stardard phosphoramidite chemistry on an automated synthesizer (Milligene Expedite). All of the reagents required for oligonucleotide synthesis were purchased from Glen Research.

The 3′-propylthiol capped oligonucleotides were prepared using 3′-Thiol-Modifier C3 S-S CPG solid supports. For the 5′-hexylthiol capped oligonucleotides, the detritylated oligonucleotide derivative on CPG supports was first prepared on the synthesizer, followed by a manual synthesis procedure reported previously to couple the 5′-thiol moiety to the oligonucleotides using 5′-Thiol-Modifier C6 S-S phosphoramidite.[10]

The oligonucleotides were cleaved from the CPG supports by incubation in 1 mL of NH$_4$OH (33% v/v) for 16 h at 55 °C. After the evaporation of ammonia under N$_2$, the crude DNA ($\sim$0.1 mL) was extracted, followed by washing of the CPG beads three times (0.3 mL of H$_2$O each). The collected crude DNA ($\sim$1 mL) was filtered with a 0.2 μm AcetatePlus syringe filter (Fisher Scientific), purified by reversed-phase HPLC on a Hewlett-Packard (HP) series 1100 system (10 × 250 mm Varian DYNAMAX C18 column, 0.03 M triethylammonium acetate (TEAA) pH 7.0 buffer, and a 1% per min gradient of 95% CH$_3$CN/5% 0.03 M TEAA at a flow rate of 3 mL/min). The retention time for the desired products is $\sim$30 min.

After HPLC purification, except for the 5′-hexylthiol-modified oligonucleotides, the 5′-termini of the target and 3′-propylthiol oligonucleotides were still protected by dimethoxytrityl (DMT) groups. To remove the DMT group, DNA strands which were dried in multiple Eppendorf tubes under vacuum were collected into one tube, and the volume was reduced to $\sim$0.2 mL under vacuum. Glacial acetic acid (0.8 mL) was added, and the solution was allowed to stand for 0.5 h and then dried under vacuum. The yellow oily products containing deprotected DNA and DMT were redissolved in $\sim$0.5 mL of H$_2$O. DMT was extracted from aqueous DNA solution using ethyl acetate (three times, 0.5 mL each); finally, residual ethyl acetate was purged by N$_2$ for 10 min. The purified DNA ($\sim$0.5 mL) was stored in a refrigerator (-20 °C).

The concentrations of the probe and target oligonucleotides were calculated on the basis of the molar extinction coefficient of single-stranded DNA[55] and the measured extinction value at 260 nm by UV−vis spectroscopy (Jasco V530).

Functionalization of Au Nanoparticles. For most of the experiments in this work, Au nanoparticles (13 nm diameter), prepared by citrate reduction of HAuCl$_4$,[56] were used. To investigate the effect of nanoparticle size on the melting properties, Au nanoparticles with average diameters of 13, 31, and 50 nm were selected. The latter two were purchased from BBI Laboratories (Burlingame, CA). The particle concentrations were determined to be approximately 15, 0.2, and 0.1 nM, respectively, for the 13, 31, and 50 nm Au colloids.

Before DNA loading, the thiol functionality on the probe oligonucleotides was deprotected. The 3′-thiol DNA was deprotected by soaking in 0.1 M dithiolthretol (DTT) in pH 8, 0.17 M phosphate buffer for at least 2 h (typically, 10 OD of concentrated DNA; 40 μL of DTT). The 5′-thiol DNA was deprotected by 50 mM AgNO$_3$ aqueous solution (typically 10 OD of concentrated DNA; 15 μL of AgNO$_3$), allowing it to stand for 20 min, followed by addition of 15 μL of DTT (10 mg/mL) to remove excess AgNO$_3$ (reaction time $\sim$5 min), and precipitates were removed by centrifuge. Aliquots of deprotected DNA solution were purified through a desalting NAP-5 column (Sephadex G-25 medium, DNA grade, Pharmacia Biotech), and the effluents from 0.5 to 1 mL were collected.

Au nanoparticles were functionalized by derivatizing aqueous Au colloid with deprotected thiol-oligonucleotides (final concentration of oligonucleotides 2−3 μM). After $\sim$16 h, the colloid solution was brought to 10 mM of phosphate (NaH$_2$PO$_4$/Na$_2$HPO$_4$) buffer by adding

0.1 M pH 7 concentrated buffer. In the subsequent salt aging process, colloids were first brought to 0.05 M of NaCl by dropwise addition of 2 M NaCl solution and allowed to stand for 6−8 h, were next salted to 0.1 M and allowed to age for another 6−8 h, were then salted to 0.2 M for standing 6−8 h, and were finally salted to 0.3 M NaCl. To remove excess thiol-DNA, the solution was centrifuged using 1.5 mL Eppendorf tubes (Fisher Scientific) (30 min at 15 000 rpm for Au 13 nm, 20 min at 8000 rpm for Au 31 nm, and 15 min at 4000 rpm for Au 50 nm). Following removal of the supernatant, the oily precipitate was then washed with 0.3 M NaCl, pH 7, 10 mM phosphate buffer solution (for simplicity, designated as 0.3 M PBS below), recentrifuged, and redispersed in 0.3 M PBS. After being washed two times, the colloid was resuspended in 0.01% azide, 0.3 M PBS, and stored in a refrigerator (4 °C).

Functionalization of Glass Substrates. The 250−300 μm diameter glass beads (Polysciences) were functionalized with capture DNA (sequence **a**, Table 1) following a modified literature method.[57] Briefly, glass beads (2 g) were first immersed in 15 mL of piranha solution (1:3 (v/v) 30% H$_2$O$_2$:H$_2$SO$_4$, **CAUTION**: strongly corrosive) in a glass Petri dish for 15 min and were then rinsed with plenty of Nanopure water (all references to H$_2$O are Nanopure, resistance $\geq$18.1 MΩ). Cleaned glass substrates were then immerged in 15 mL of a solution of 1% 3-aminopropyltrimethoxysilane (APS, Aldrich) and 0.01% glacial acetic acid in H$_2$O in a polystyrene dish and were rotated on an orbital shaker for 30 min at room temperature. The silane-modified glass substrates were then washed three times with H$_2$O, dried under N$_2$, and baked in an oven at 120 °C for 10 min, followed by prompt treatment of the substrate surface with 10 mL of 1 mM succinimidyl 4-(maleimidophenyl) butyrate (SMPB, Sigma) in a 4:1 (v/v) EtOH: DMSO solution in a glass dish, allowing at least 2 h for coupling, and were rinsed three times with EtOH and dried under N$_2$. Coupling of freshly deprotected thiol-DNA to the SMPB-modified glass surface was carried out using 2 μM thiol DNA in 0.1 M PBS solution; the reaction was allowed to proceed overnight at room temperature, and was then rinsed three times with 0.3 M PBS and stocked in PBS buffer for the hybridization experiments.

Hybridization of Nanoparticles with Targets in the Solution System. The molar concentrations of Au particle probes were measured by UV−vis spectroscopy (molar extinction coefficients are 2.7 × 10^8 M^{-1} cm^{-1} at λ_{520} for 13 nm particles, 3.7 × 10^9 M^{-1} cm^{-1} at λ_{528} for 31 nm particles, and 1.5 × 10^{10} M^{-1} cm^{-1} at λ_{540} for 50 nm particles, respectively).

Two sets of DNA-functionalized Au nanoparticles (probes **a** and **b** in 0.3 M PBS, 1.5 pmol of each for Au 13 nm particles, 50 fmol of each for Au 31 nm, and 25 fmol of each for Au 50 nm) were mixed at a 1:1 ratio, and target DNA was added to the solution of probes (60, 5, and 1 pmol target for Au 13, 31, and 50 nm particles, respectively). The total volume of the mixed solution was adjusted to 1 mL using 0.3 M PBS. Note that in the salt-dependent experiments, various salt concentrations were used in the hybridization buffer. The solution was then heated to $\sim$70 °C (above the melting point) for 5−10 min, and was then allowed to cool to room temperature. After $\sim$2 h, macroscopic nanoparticle aggregates formed, and a red to purple color change of the solution was observed. The color change can be enhanced by spotting 5 μL of the nanoparticle solution before and after DNA hybridization onto a C18 reversed-phase TLC plate (spot test).[10]

Hybridization of Nanoparticles on Oligonucleotide-Modified Glass Surfaces. Glass substrates (250−300 μm diameter beads, 0.25 g for each melting experiment), modified with capture strands, were immersed in a solution containing target oligonucleotides (60 nM, 0.3 M PBS) for 4 h to allow target hybridization with capture strands. The solution containing unreacted target was removed, and the substrates were washed three times with 0.3 M PBS. Au nanoparticle probes (5

(55) http://basic.nwu.edu.
(56) Freeman, R. G.; Hommer, M. B.; Grabar, K. C.; Jackson, M. A.; Natan, M. J. *J. Phys. Chem.* **1996**, *100*, 718.

(57) Chrisey, L. A.; Lee, G. U.; O'Ferrall, C. E. *Nucleic Acids Res.* **1996**, *24*, 3031.

nM for Au 13 nm, 0.2 nM for Au 31 nm, and 0.1 nM for Au50 nm) were then hybridized to the unhybridized portion of the target bound on the glass substrate (reaction time 2 h at room temperature). Excess nanoparticle probes were then removed, and the glass substates bearing the Au nanoparticles were washed three times with 0.3 M PBS, and then soaked in 0.3 M PBS for the melting analysis.

Melting Analyses. To improve the reproducibility of the melting analysis, one batch of Au nanoparticle, target, hybridization buffer, and glass beads (divided into several portions) was used for all experiments. The standard deviation for T_m is less than ±0.3 °C for the solution aggregate system, and $\pm(0.5-1)$ °C for the glass bead system. The melting analyses were carried out using a HP 8453 diode array spectrophotometer equipped with a HP 89090a Peltier temperature controller (Hewlett-Packard). The melting process was monitored by measuring the change in extinction at 260 nm or the λ_{max} for the Au nanoparticles (520, 528, and 540 nm for 13, 30, and 50 nm Au particles, respectively). For the homogeneous system, the aggregate suspension was stirred continuously with a magnetic stir bar at 460 rpm as the solution temperature was increased from 20 to 70 °C at 0.5 °C intervals with a holding time of 1 min at each point prior to each spectroscopic measurement. The data for the melting curve were processed by a linear insertion at 0.1 °C divisions. The first derivative generated from the melting curves using the instrument software was used to determine the T_m and sharpness as measured by the full width at half-maximum (fwhm).

For the glass surface system, as with the solution melting experiments, extinction measurements were recorded at 0.5 °C intervals from 25 to 70 °C, with a holding time of 1 min at each temperature point. Because the $250-300$ μm glass beads are not suspended in the solution, agitation by manual shaking of the cuvette prior to UV–vis measurement was performed to ensure homogenization of the solution; before each measurement was taken, the beads were allowed to settle out of the UV–vis beam path for 30 s.

Transmission Electron Microscopy. TEM images of DNA-functionalized Au nanoparticles were obtained on a Hitachi 8100 transmission electron microscope. Samples were prepared by pipetting 5 μL of colloid solution onto a carbon-coated copper grid (200 mesh, Ted Pella). After the evaporation of solvent, the grid was dried overnight under vacuum. The TEM operating voltage was 200 kV, and the filament current was 10 μA. All of the images are bright-field images.

Circular Dichroism. Circular dichroism (CD) experiments were performed on a Jascol 700 Spectropolarimeter (Jasco Corp.) equipped with a Peltier temperature controller. The melting curve was recorded by monitoring the CD signal of the sample over a $20-75$ °C temperature range with a 0.5 °C increment step. After equilibration at each temperature, CD measurements were averaged over a 30 s period. The parameters for the spectrometer are 2 nm of spectral bandwidth and 10 mdeg sensitivity.

Supporting Information Available: TEM images of oligo-nucleotide-functionalized Au nanoparticles with diameters of 13, 31, and 50 nm (PDF). This material is available free of charge via the Internet at http://pubs.acs.org.

JA021096V